Society For Biomaterials

Morphology and surface properties of high strength siloxane poly(urethane-urea)s developed for heart valve application

Loshini S. Dandeniyage,[1,2] Raju Adhikari,[2] Mark Bown,[2] Robert Shanks,[1] Benu Adhikari,[1,2] Christopher D. Easton,[2] Thomas R. Gengenbach,[2] David Cookson,[3] Pathiraja A. Gunatillake[2]

[1]School of Science, RMIT University, Melbourne, City campus, Victoria 3000, Australia
[2]CSIRO Manufacturing, Clayton, Victoria 3168, Australia
[3]Australian Synchrotron ANSTO, Clayton, Victoria 3168, Australia

Received 12 November 2017; revised 28 January 2018; accepted 12 February 2018
Published online 00 Month 2018 in Wiley Online Library (wileyonlinelibrary.com). DOI: 10.1002/jbm.b.34101

ABSTRACT: A series of siloxane poly(urethane-urea) (SiPUU) were developed by incorporating a macrodiol linked with a diisocyanate to enhance mixing of hard and soft segments (SS). The effect of this modification on morphology, surface properties, surface elemental composition, and creep resistance was investigated. The linked macrodiol was prepared by reacting α,ω-bis(6-hydroxyethoxypropyl) poly(dimethylsiloxane)(PDMS) or poly(hexamethylene oxide) (PHMO) with either 4,4′-methylenediphenyl diisocyanate (MDI), hexamethylene diisocyanate (HDI), or isophorone diisocyanate (IPDI). SiPUU with PHMO-MDI-PHMO and PHMO-IPDI-PHMO linked macrodiols showed enhanced creep resistance and recovery when compared with a commercial biostable polyurethane, Elast-Eon™ 2A. Small and wide-angle X-ray scattering data were consistent with significant increase of hydrogen bonding between hard and SS with linked-macrodiols, which improved SiPUU's tensile stress and tear strengths. These SiPUU were hydrophobic with contact angle higher than 101° and they had low water uptake (0.7%·w/w of dry mass). They also had much higher siloxane concentration on the surface compared to that in the bulk. © 2018 Wiley Periodicals, Inc. J Biomed Mater Res Part B: Appl Biomater 00B: 000–000, 2018.

Key Words: poly(urethane-urea), morphology, polydimethylsiloxane, linked-macrodiol, biostable

How to cite this article: Dandeniyage LS, Adhikari R, Bown M, Shanks R, Adhikari B, Easton CD, Gengenbach TR, Cookson D, Gunatillake PA 2018. Morphology and surface properties of high strength siloxane poly(urethane-urea)s developed for heart valve application. J Biomed Mater Res Part B 2018;00B:000–000.

INTRODUCTION

Thermoplastic segmented polyurethanes (PU) and poly(urethane-urea)s (PUU) have found applications in a range of biomedical applications[1–4] due to their exceptional biocompatibility, stability, and mechanical performance. Segmented PU are composed of chemically bonded alternating soft and hard segments. The soft segment (SS) provides a continuous matrix with flexibility having a glass transition temperature (T_g) well below the use temperature. The rigid hard segment is dispersed in the SS matrix performing as physical crosslinks. It has T_g and melting temperature (T_m) above the temperature range of their application. Incompatibility of hard and SS creates a microphase separated morphology[5–7] affecting the mechanical properties and biostability of the PU.

Microphase separation depends on several factors such as molecular weight of the SS,[8] structure of comacrodiol,[9] chain extender composition,[10,11] intermolecular hydrogen bonding between hard and SS,[12] compatibility between hard and SS, and processing conditions.[13] A thorough understanding of these attributes will be needed to optimize for target biomedical applications.

It is well established that the incorporation of siloxane segments as part of the PU structure enhances long-term biostability. Siloxane polyurethanes (SiPU) and siloxane poly(urethane-urea)s (SiPUU) have shown promising results in many medical implants.[14–17] However, this improvement comes with a compromise in mechanical properties. The mechanical properties of PU are influenced by micro-phase separation of polar hard segments and nonpolar SS triggered by their incompatibility. Use of highly nonpolar macrodiols, such as poly(dimethylsiloxane) in the SS results in highly phase-separated PU due to poor miscibility with polar hard segment.[18] The relative difference in solubility parameters of various segments forming a polyurethane is a good guide to assess the extent of phase separation. For example, the solubility parameters of poly(dimethylsiloxane), urethane and urea groups, respectively are (15.5 $J^{1/2}$ $cm^{-3/2}$), (37.2 $J^{1/2}$ $cm^{-3/2}$) and (45.6 $J^{1/2}$ $cm^{-3/2}$).[19] Typically the PU prepared from these components are highly phase separated and consequently have poor mechanical properties. The use of a mixture of poly(dimethylsiloxane) end-capped with hydroxyl-ethoxy propyl groups and less

Correspondence to: P. A. Gunatillake; e-mail: thilak.gunatillake@csiro.au
Contract grant sponsor: Frank McGuire, the Chief Executive of Foldax Inc

TABLE I. Abbreviations for SiPUU with Different Linked-Macrodiols in the Soft Segment, Number Average Molecular Weight (M_n) and Polydispersity Index (PDI)

Abbreviation for SiPUU	Soft Segment Component		M_n (g/mol)	PDI
	PDMS or Linked PDMS	PHMO or Linked PHMO		
PU-C	PDMS	PHMO	117,489 ± 2163	3.8 ± 0.02
PU-1	PDMS	PHMO-MDI-PHMO	128,863 ± 6669	3.0 ± 0.7
PU-2	PDMS-MDI-PDMS	PHMO	102,349 ± 4934	3.3 ± 0.4
PU-3	PDMS	PHMO-HDI-PHMO	100,633 ± 7333	3.0 ± 0.05
PU-4	PDMS-HDI-PDMS	PHMO	105,238 ± 7905	3.7 ± 0.4
PU-5	PDMS	PHMO-IPDI-PHMO	96,560 ± 6210	3.2 ± 0.1
PU-6	PDMS-IPDI-PDMS	PHMO	87,983 ± 4099	2.4 ± 0.06

hydrophilic poly(hexamethylene oxide) (PHMO) has enabled the synthesis of materials with good mechanical properties. The inter domain region between hard and SS formed by PHMO and end groups provide compatibilization between apparently incompatible hydrophilic and hydrophobic segments.[20]

We recently reported the synthesis and mechanical properties of a series of SiPUU, designed specifically for applications such as synthetic heart valves requiring high mechanical strength.[21,22] In this study, we investigated the introduction of polar functional groups to the SS by linking macrodiols with diisocyanate linkers. This approach enabled us to prepare SiPUU with high tensile and tear strengths, and high resistance to creep deformation. The linking of macrodiols with polar functional groups to increase intermolecular hydrogen bonding, and the use of mixed macrodiols and mixed chain extenders resulted in materials with morphologies significantly different to those conventional PU, which exhibit two-phase microstructure. The microstructural organization of various segments influences the mechanical properties, susceptibility of functional groups to degradation as well as the chemical composition of the material surface.

We found few literature reports on studies to investigate the morphology and surface properties of PU based on mixtures of chemically different macrodiols. Hernandez et al. reported that PU based on a mixture of α,ω-bis(6-hydroxyethoxypropyl) poly(dimethylsiloxane) (PDMS) and PHMO (80/20) macrodiols (Elast-Eon™ 2A) have a three-phase, core-shell morphology.[20] The PDMS SS exhibited a single phase while the ethoxy-propyl end groups formed a second phase with the PHMO. The third phase was formed by 4,4′-methylenediphenyl diisocyanate (MDI)–butanediol (BDO) based hard segment. Modeling studies supported the existence of tri-phase morphologies in thermoplastic PU based of two chemically different SS.[23] As a siloxane polyurethane, Elast-Eon™ 2A is arguably the most biostable polyurethane with good mechanical properties and biostability confirmed by over 10 years of successful clinical data. Hence, we have reported the properties of new materials in this study compared to Elast-Eon™ 2A.

Herein we report the creep and recovery, morphology, and surface properties of a series of SiPUU developed for application in synthetic heart valves. These properties are useful to the characterization of the long-term functional performance of the synthetic heart valve leaflets.

MATERIALS AND METHODS

PDMS and PHMO mixed-macrodiol based (80:20 w/w ratio) SiPUU were used in these experiments. Either PHMO (713 g/mol) or PDMS (998 g/mol) was linked with one of the diisocyanates, 4,4′-methylenediphenyl diisocyanate (MDI), hexamethylene diisocyanate (HDI), or isophorone diisocyanate (IPDI) to introduce a polar functionality to the SS (except the control). Hard segment of all SiPUU were composed of MDI and 50:50 (molar ratio) mixture of 1,3-*bis*(4-hydroxybutyl)-1,1,3,3-tetramethyldisiloxane (BHTD) and 1,2-ethylenediamine (EDA). The hard segment composition was maintained constant at 45%·w/w of the total mass. The synthesis process of these SiPUU using two-step solution polymerization in DMAc, film casting and mechanical testing of these SiPUU series were described in detail in our earlier work.[22] Solvent cast films were used for all the subsequent experiments. Cast films were stored in a desiccator at room temperature for a week before the testings. Elast-Eon™ 2A (denoted here as E2A) was received from Abbott, MN (formerly St Jude Medical, St Paul, MN). E2A is a polyurethane in which the SS is formed from a mixture of PDMS and PHMO (80:20) and the hard segment from MDI and BDO.[24] Table I shows molecular weights and dispersity of the synthesized SiPUU, the SS composition and relevant abbreviation of SiPUU referred to this discussion. The dispersity was broad for all SiPUU presumably due to extremely fast reaction of amine groups with isocyanate in the final step of the polymerization.

Characterization of SiPUU

Creep and recovery tests were performed using Q800 DMA (TA instruments, New Castle, DE) with rectangular specimens (0.2–0.5 mm thickness) under tensile mode at 25°C. Creep tests were conducted over 60 min followed by recovery time of 120 min under 2 MPa applied stress.

Specimens were analyzed using a Zeiss Merlin field emission scanning electron microscope (FESEM) (Carl Zeiss Microscopy, Jena, Germany) operated in secondary electron and backscatter modes. Energy dispersive X-ray (EDX) analysis was carried out using an Oxford Instruments 80 mm^2

SSD detector. An accelerating voltage of 3 kV was used for imaging and EDX analysis at a working distance of 4.0 mm. This voltage was selected based on the properties of the polyurethane tested. All the specimens were coated with iridium and mounted on aluminum stubs with carbon conductive paint.

X-ray photoelectron spectroscopy (XPS) depth profiles employing a gas cluster ion source were used to determine the variation of elemental composition of the SiPUU from surface to bulk. XPS analysis was performed using an AXIS Nova spectrometer (Kratos Analytical, Manchester, UK) with a monochromated Al Kα source. The total pressure in the main vacuum chamber during analysis was typically between 10^{-9} and 10^{-8} mbar. Survey spectra were acquired at a pass energy of 160 eV. To obtain more detailed information about chemical structure, high resolution spectra were recorded from individual peaks at 40 eV pass energy (yielding a typical peak width for polymers of 0.9–1.0 eV). Depth profiling experiments were conducted using a Minibeam 6 Ar Gas Cluster Ion Source (GCIS, Kratos Analytical) operated at a cluster size of Ar500+ and impact energy of 10 keV, equating to a partition energy of 20 eV per atom. For the ion beam a raster size of 2 × 2 mm was used for all etching experiments.

A Bruker Dimension Fast Scan atomic force microscope (AFM) with Icon scanning head and NanoScope 9.1.3 software (Bruker Corporation, Billerica, MA) was used to measure surface topography of SiPUU films in PeakForce QNM mode. Ultrasharp silicon nitride tips were used to image under ambient (ScanAsyst-Air) and hydrated (ScanAsyst-Fluid) conditions. Scans of 1 × 1 μm^2 were performed at 0.8 Hz and 512 data per scan line, at an aspect ratio of 1, 2, or 4. For images collected under hydrated conditions, a small amount of MilliQ™ water was first placed on the surface and left for at least 30 min to equilibrate; then a small drop of MilliQ™ water was placed on the probe to facilitate engaging the surface in water. All images were flattened using NanoScope Analysis 1.5 software.

Small-angle X-ray scattering (SAXS) and Wide-angle X-ray scattering (WAXS) data were collected on the SWAXS beamline at the Australian Synchrotron. SAXS (WAXS) measurements were performed in transmission geometry with a sample-to-detector distance of 3343 mm (561 mm) and an irradiation wavelength of 0.151 nm (0.062 nm). Each 2D image was azimuthally integrated to give a 1D profile of scattering intensity versus 2θ or q where $q = 4\pi\sin\theta/\lambda$ corresponding to a scattering angle 2θ and X-ray wavelength λ. All the SAXS and WAXS profiles shown are the result of averaging 11 profiles taken at 100 μm increments across the polymer surface. All the WAXS data were normalized to constant integrated scattering intensity (integrated from $q = 4$ to 25 nm^{-1}). This normalization factor was applied to SAXS data collected at the corresponding sample locations.

Wettability and water uptake analysis

Water contact angle (CA) measurements of SiPUU and E2A films were determined using CAM200 tensiometer (KSV Instruments, Helsinki, Finland) connected to a A602i high-resolution digital camera (Basler AG, Ahrensburg, Germany). The measurements were obtained by placing a single drop of MilliQ™ water on the sample surface at room temperature. Attension Theta SFE image analysis software was used to determine the CA values. An average of three replicates in different areas of the polymer sample is reported.

Water uptake analysis was performed gravimetrically in accordance with ASTM D5229. Samples were cut into 20 × 10 mm^2 rectangular shaped specimens in the thickness range 0.5–0.7 mm. Five specimens were used for each sample. Specimens were dried at 80°C under 0.1 mbar to constant weight. This weight was used as the baseline weight (W_b). Dry specimens were immersed completely in a water bath at 37°C. After a specific time interval the specimens were removed from the water bath and put into separate specimen bags and kept in the desiccator to cool to room temperature. Excess surface moisture was wiped using a Kimwipe™, the specimens were weighed immediately and returned to the water-bath. The procedure was continued until the weight of the specimen remained constant and this weight was taken to be the final weight (W_f).

$$\text{Mass change}\,(\%) = \frac{(Wf - Wb)}{Wb} \times 100 \quad (1)$$

RESULTS

Mechanical properties

Of the six SiPUU in the series, PU-1 and PU-5 exhibited tensile strength over 30 MPa and elongation over 600% while the Young's modulus was <20 MPa, suitable properties for fabrication of synthetic heart valve leaflets.[22]

Creep and recovery

Figure 1 shows the creep and recovery strain of SiPUU and E2A as a function of time. Primary and secondary creep stages can be clearly observed in synthesized SiPUU. In recovery phase, instantaneous recovery is rapid for all SiPUU and E2A with recovery time <0.5 s. Subsequently the recovery rate slowed for viscoelastic component due to time-dependent molecular relaxation [Figure 1(a)]. However, PU-1 has the highest recovery of strain when compared with E2A [Figure 1(b)].

Surface elemental composition

The elemental composition [Si, O, N, and C] of the SiPUU obtained from scanning electron microscope-energy dispersive X-ray (SEM-EDX) analysis in the penetration depth of 1–2 μm are presented in Table II. The corresponding calculated elemental compositions (according to the empirical formula) of these materials as formulated are also presented for comparison. Higher amount of Si was measured than the calculated value for all the polymers except PU-3. SiPUU with MDI linked polyol showed a higher Si content than those linked with either HDI or IPDI.

Figure 2 illustrates Si and N mapping of SiPUU series using SEM-EDX analysis in 1–2 μm depth from the surface at 5000× magnification. PU-1 shows more Si concentration

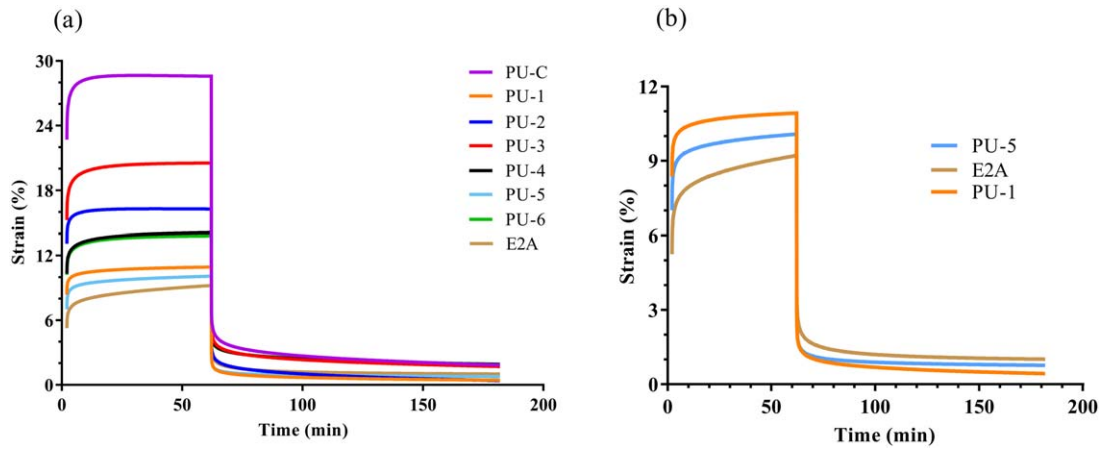

FIGURE 1. Creep and recovery strain-time curve of (a) SiPUU series, (b) PU-1, PU-5, and E2A. Sixty minute creep test was conducted under 2 MPa stress followed by 120 min recovery at 25°C.

while PU-6 shows the least Si accumulated correlating with the measured Si composition of Table II.

Figure 3 shows the XPS depth profiles of atomic concentrations of C, N, O, and Si elements as a function of etch time. The composition at zero etch time represents the top surface of each SiPUU, increasing etch time corresponds to increasing depth below the surface. Actual etch rates could not be determined as it was impossible to prepare well-defined calibration samples because of the problems related to solubility of our materials. However, in the case of other PDMS-based copolymer studied in our lab etch rates of 0.2–0.5 nm/s (12–30 nm/min) were obtained under identical experimental conditions. For all SiPUU in the series the top surface layer was found to be enriched in Si. Table III shows the Si% of the top surface of each SiPUU.

AFM analysis

AFM height channel (Figure 4) shows the surface topography of the material. Brighter and darker regions represent hills and troughs respectively, as represented by the *Z*-scale color bar to the right of each image. E2A shows more spherical-like nanosized features in atmosphere height channel and there is no apparent change when hydrated. However, when hydrated PU-C and PU-1 lost the nanostructure that was present in atmosphere and we only see some micron-sized undulations. The adhesion channel (Figure 5) shows the force required to remove the tip from the surface, with brighter to darker areas demonstrate contrast in adhesion. The adhesion channels are similar for all three materials in air and when they are hydrated. However, PU-1 shows to be less sticky than PU-C in hydrated condition, based on a comparison of the amount of dark regions in the two adhesion channel (i.e., there is a greater amount of dark region for the PU-1 adhesion channel when hydrated).

X-ray scattering analysis

Figure 6(a,b) present the SAXS intensity profiles of the SiPUU and E2A. The chemical composition of hard segment is common for all the SiPUU in this series. However, larger interdomain spacing is observed in PU-2, PU-4, and PU-6,

TABLE II. Calculated (from the Formula) and Measured (Using SEM–EDX) Elemental Composition of C, O, N, and Si in SiPUU

		Element (%)				Difference of the Measured Composition (%)	
SiPUU		C	O	N	Si	N	Si
PU-C	Calculated	54.2	17.7	4.7	15.6		
	Measured	57.3	18.7	4.5	19.6	0.2↓	4.0↑
PU-1	Calculated	54.2	17.7	4.8	15.7		
	Measured	50.9	24.3	4.1	20.8	0.7↓	5.1↑
PU-2	Calculated	56.9	18.1	5.2	15.4		
	Measured	57.6	19.7	5.0	17.6	0.2↓	2.2↑
PU-3	Calculated	53.9	17.7	4.9	15.7		
	Measured	61.7	17.2	6.4	14.8	1.5↑	0.9↓
PU-4	Calculated	54.3	17.6	5.2	15.0		
	Measured	59.9	17.6	6.0	16.5	0.8↑	1.5↑
PU-5	Calculated	53.9	17.7	4.8	15.7		
	Measured	60.1	17.9	5.1	16.9	0.3↑	1.2↑
PU-6	Calculated	54.8	17.4	5.2	14.6		
	Measured	61.8	17.0	6.4	14.8	1.2↑	0.2↑

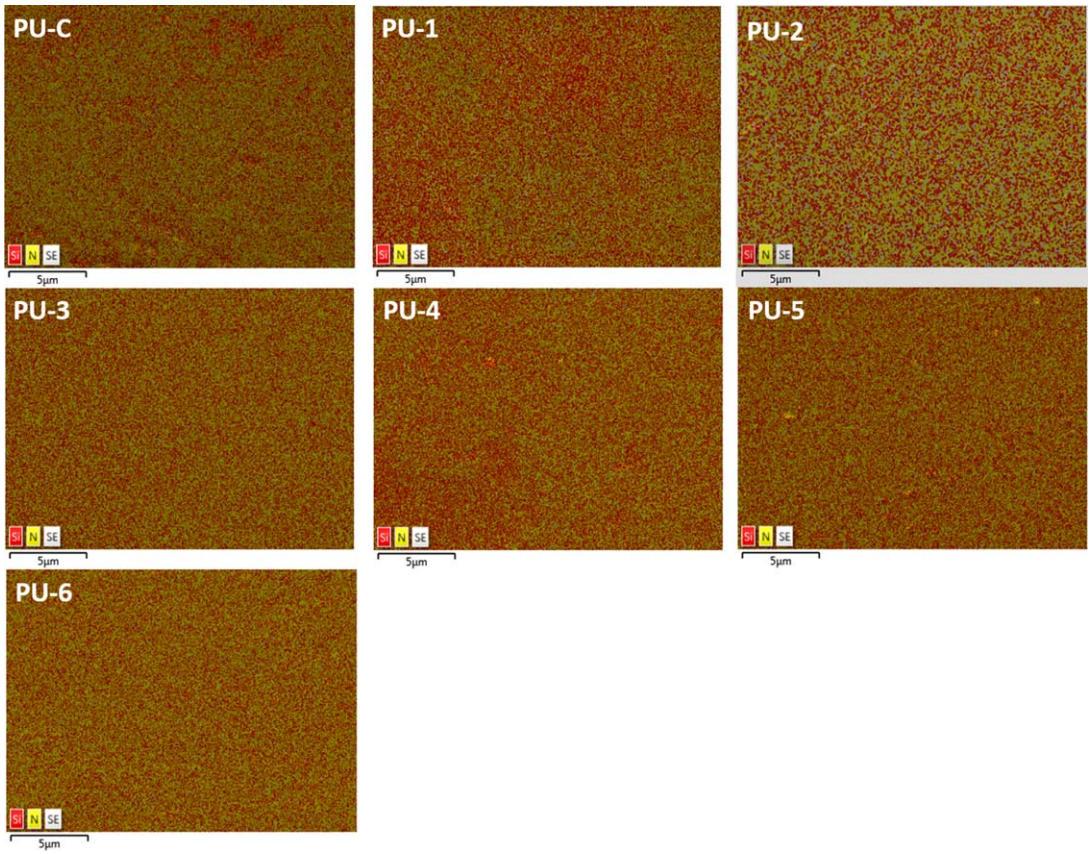

FIGURE 2. SEM–EDX layered images for Si (red) and N (yellow) mapping of SiPUU at 1–2 μm depth from the surface.

which contain PDMS-MDI-PDMS, PDMS-HDI-PDMS, and PDMS-IPDI-PDMS linked macrodiols, respectively. In contrast, SiPUU comprised of PHMO-linked macrodiols and the control (PU-C) show an interdomain spacing similar to E2A.

Figure 7(a,b) show the WAXS of SiPUU series and E2A respectively. All the SiPUU and E2A show the first peak at $2\theta \approx 12.5°$. The peak at $2\theta \approx 20°$ is also visible for both E2A and SiPUU, although for the latter the broad peaks appear to have some narrower peaks superimposed upon them at scattering angles including 6°, 12°, 16° 20°, 24°, and 31°.

Water uptake and wettability characteristics

Table IV shows the water contact angle of SiPUU and E2A at 30 s. The results show that the CA of SiPUU and E2A ranged from 101.7° to 113.9°. As shown in Figure 8, all the SiPUU in the series (except PU-3) absorbed 0.62–0.70% water within 2 h and it was constant for the next 3 and 4 h. Water uptake of SiPUU is comparable to that of E2A.

DISCUSSION

Creep and recovery

Creep is time-dependent deformation of viscoelastic materials under constant stress over time and recovery is the ability to recover the deformation (or strain) once the stress is removed, a common phenomenon of viscoelastic materials. This is an important parameter for a material used in synthetic heart valves as it is related to the proper functioning of the valve over many millions of open-close cycles. The slope of the strain-time curve gives the creep rate.[25] It can be seen that the creep strain of PU-1 and PU-5 are higher than E2A [Figure 1(b)]. This implies that PU-1 and PU-5 show better resistance to creep deformation when compared with E2A, presumably due to increased intermolecular attractions associated with the diisocyanate linking of the PHMO phase.

In a polymeric material instantaneous recovery strain represents the elastic component of the polymer and unrecoverable strain represents the plastic component.[26] All the polymers show 70% and higher instant elastic recovery with sharp decrease in the strain after removing the stress [Figure 1(a)]. Creep-recovery depends strongly on the morphology of the material and unrecoverable strain corresponds to permanent deformation of the molecular structure due to chain slipping.[27] E2A and PU-C show the highest unrecoverable strain than the other SiPUU formulations while PU-1 has the lowest. This can be attributed to the urethane linkages of the linked macrodiols in the SS of SiPUU, as well as the urea linkages present in the hard segment. In PU-1 to PU-6, urethane linkages in the SS are likely to form stronger hydrogen bonding with urethane and urea linkages in the hard segment compared to E2A and PU-C. These strong interactions may reduce the amount of molecular chain slippage responsible for permanent deformation.

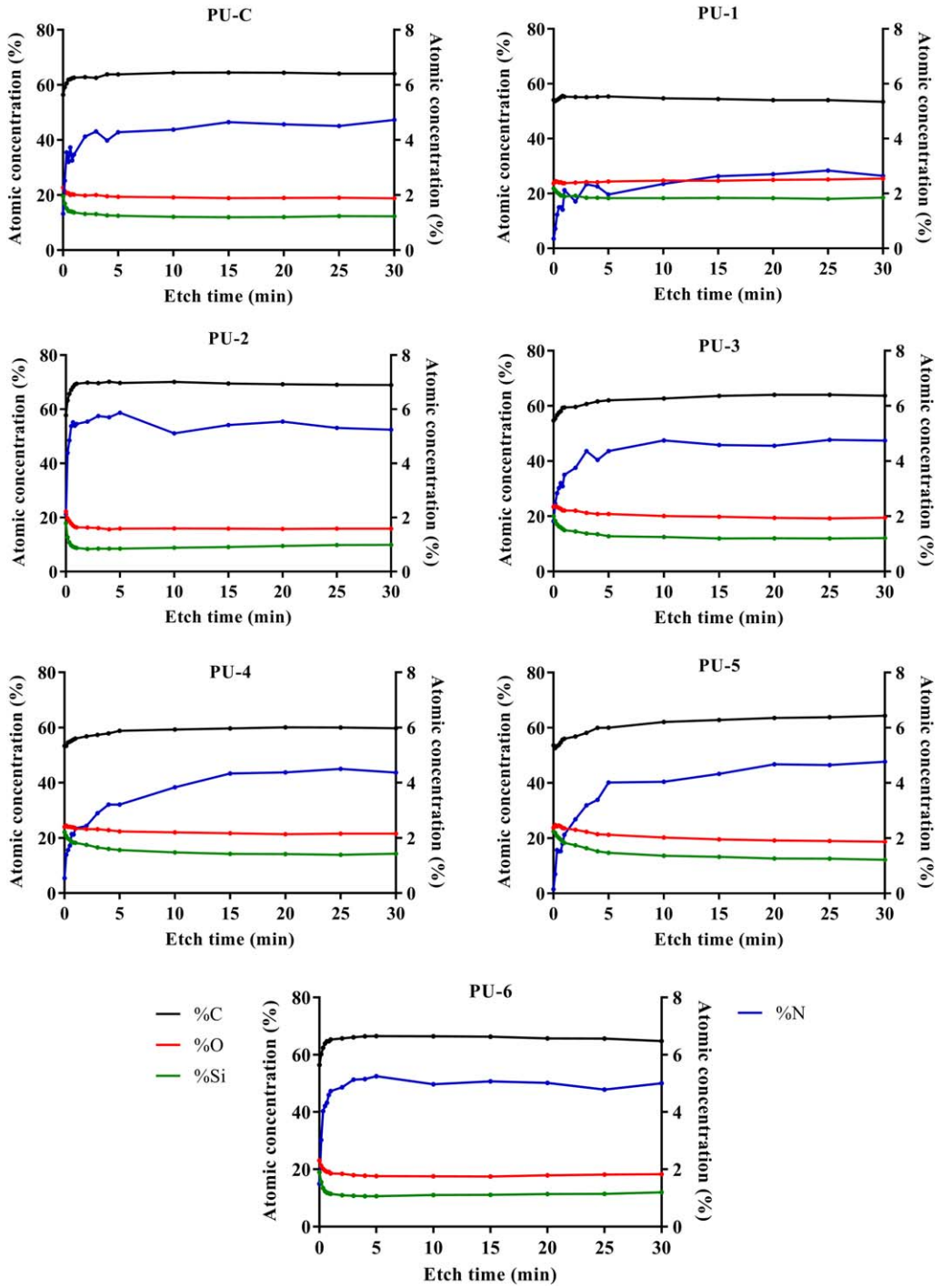

FIGURE 3. Compositional depth profiles of atomic concentrations of C, N, O, and Si in SiPUU verses etch time. Zero second etch time represents the top surface and increasing etch time corresponds to increasing depth below the surface. Left *y*-axis gives the C%, O%, Si%, and right *y*-axis gives N%.

TABLE III. XPS Data for Si% of Top Surface of SiPUU (0 s Etch Time) in Comparison to Calculated Si% (Bulk)

SiPUU	PU-C	PU-1	PU-2	PU-3	PU-4	PU-5	PU-6
Si% at 0 s etch time	19.5	21.8	17.9	20.0	22.1	22.4	19.0
Calculated Si% (bulk)	15.6	15.7	15.4	15.7	15.0	15.7	14.6

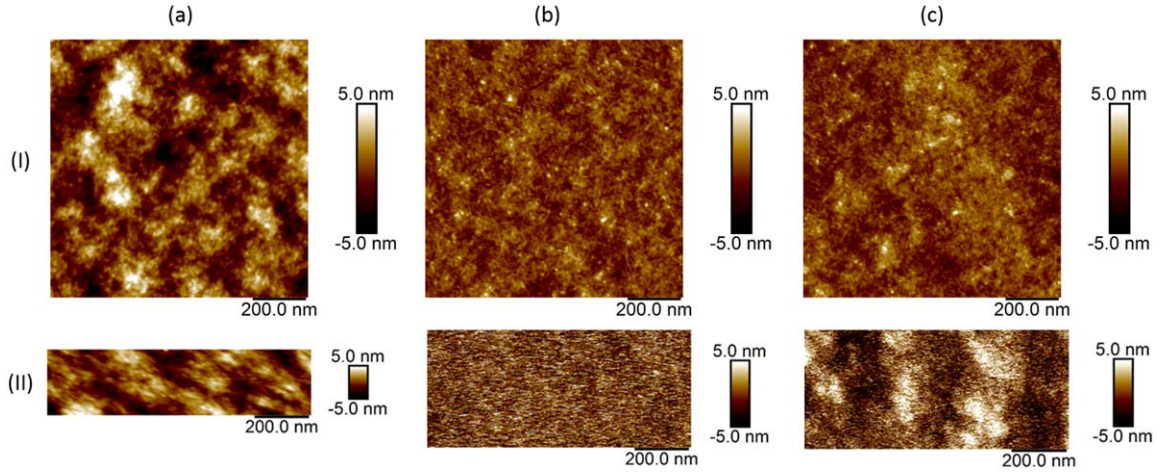

FIGURE 4. AFM height channels of (a) E2A, (b) PU-C, and (c) PU-1 in (I) air and (II) hydrated conditions.

Accumulation of silicon on the surface of SiPUU

It has been shown that the Si can migrate toward the surface due to low surface energy of siloxane segments.[28] Furthermore, SEM-EDX has been used to measure the elemental composition of SiPU on the surface.[29,30] However, due to a lack of relevant experimental details in the reported studies it is not clear whether the sample depth investigated was closer to the surface or not. In our study, based on the chosen experimental condition for SEM-EDX analysis, the measured elemental composition may be the average up to a sample depth of ~1 to 2 μm. The difference of Si between measured (by SEM-EDX) and calculated was higher for PU-C (nonlinked) and PU-1 (PHMO-linked with MDI) as shown in Table II. PU-2 also showed a higher Si content compared to the other four materials in the series. It is noted that the SiPUU with MDI linked polyol (PHMO or PDMS) showed higher Si compared to those with polyols linked with either IPDI or HDI, perhaps indicative of better phase separation in those materials. It is likely that the surface composition may change when exposed to aqueous environment or isotonic saline at 37°C.

XPS is a more suited technique to obtain surface elemental composition as it provides compositional profiles of atomic concentrations. The observed decrease of Si concentration with etch time in XPS analysis is strongly indicated the presence of a Si enriched surface and it is consistent with surface enrichment of siloxane segments reported for siloxane-based PU.[31] Table III shows a higher concentration of Si% on the surface of PU-1, PU-4, and PU-5, consistent with the SEM-EDX mapping (Figure 2) results. The Si concentration decreases as the etch time is increased along with an increase in N concentration. In summary, the SiPUU in the series show Si enriched surface in agreement with that reported for siloxane-based PU.

Morphological characteristics

AFM height and adhesion channels were used to investigate the structural changes of PU-C and PU-1 in hydrated conditions compared with E2A. The surface rearrangement of PU-C and PU-1 in hydrated conditions in AFM height channel can be expected to be due to urea linkages, which are not present in E2A. The microstructural organization of E2A has been described by core-shell model and it has been proven by AFM phase images.[20,32]

The peaks present in all SAXS profiles represents a well preserved distance in real space. It is likely that q_{max} at the

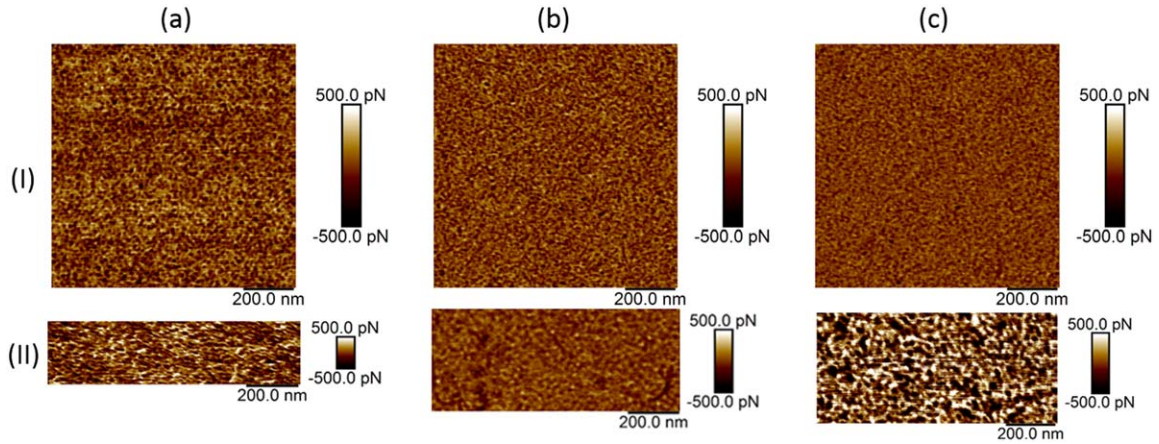

FIGURE 5. AFM adhesion channels of (a) E2A, (b) PU-C, and (c) PU-1 in (I) air and (II) hydrated conditions.

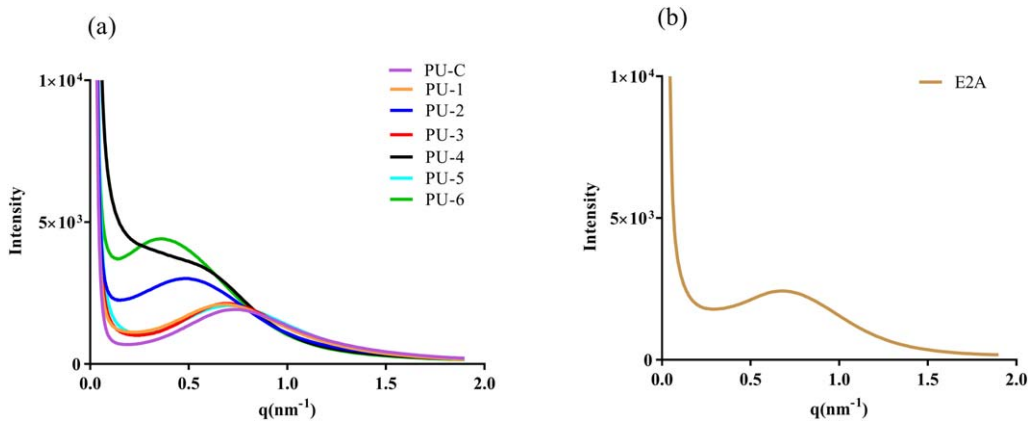

FIGURE 6. Small angle X-ray scattering (SAXS) patterns for (a) SiPUU series and (b) E2A.

centroid of this peak reflects the mean interdomain spacing (d) between the hard domains given by $d = 2\pi/q_{max}$.[33] The shifting of the peak toward $q = 0$ associated with an increase in interdomain spacing has been previously associated with increasing incompatibility and poor miscibility of hard and SS in block copolymers.[34,35] Our results show that the use of PHMO-linked macrodiols improves the phase-mixed morphology to enhance the compatibility between SS and hard segments compared to the use of PDMS-linked macrodiols. This may be the main reason for the observed improvement in mechanical properties of SiPUU synthesized using PHMO-linked macrodiol.

It has been reported that E2A shows three-phase morphology comprising of siloxane segments of PDMS, hard domain and mixed-phase of PHMO and ethoxypropyl end groups of PDMS.[20] WAXS peak at $2\theta \approx 12.5°$confirms the formation of pure PDMS phase in SiPUU, similarly as reported for mixed macrodiol-based siloxane PU.[20,36] $2\theta \approx 20°$ is typical for segmented PU and PUU and is indicative of the mean distance between non-PDMS segments. The narrower peaks of SiPUU at 6°, 12°, 16°, 20°, 24°, and 31° correspond to characteristic real space distances of 1.2, 0.68, 0.57, 0.54, 0.45, and 0.37 nm, respectively, and suggest a greater tendency for 3D ordering of the non-PDMS segments on top of an average nearest-neighbor spacing. While increased 3D ordering is a reasonable explanation for the additional peaks observed in the SiPUU WAXS, it should be noted that no single crystallographic symmetry (such as face centered cubic) can account for the positions and relative intensities of all the peaks observed.

Hydrophobicity of SiPUU

Generally, a material is considered as hydrophobic when the CA is higher than 90° and as hydrophilic when it is below 90°. High contact angles (Table IV) demonstrate that all of the SiPUU and E2A polymer surfaces are hydrophobic. SiPUU containing PHMO-MDI-PHMO linked macrodiol (PU-1) was the most hydrophobic and nonwetting polymer as observed higher amount of Si accumulated by XPS data and SEM-EDX mapping.

Synthetic, biostable, and biocompatible materials for cardiovascular applications are preferred to be more hydrophobic to minimize the biodegradation for long term functionality. It has been demonstrated that the

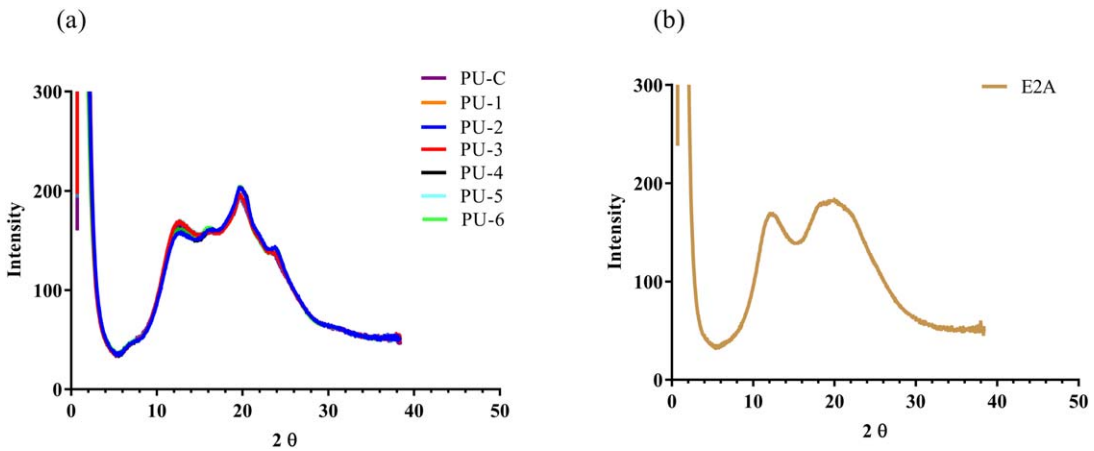

FIGURE 7. Wide angle X-ray scattering (WAXS) patterns for (a) SiPUU series and (b) E2A. Note that although this data was actually collected at $\lambda = 0.062$ nm, the angular scale shown has been transformed for an X-ray wavelength of 0.154 nm for easier comparison to previously reported work.

TABLE IV. Water Contact Angles of SiPUU Measured at 30 s

SiPUU	CA at θ_{30s} (°)
PU-C	110.1 ± 4.6
PU-1	113.6 ± 0.9
PU-2	106.6 ± 6.4
PU-3	105.3 ± 1.5
PU-4	101.0 ± 0.2
PU-5	111.6 ± 2.9
PU-6	106.0 ± 2.8
E2A	107.5 ± 0.8

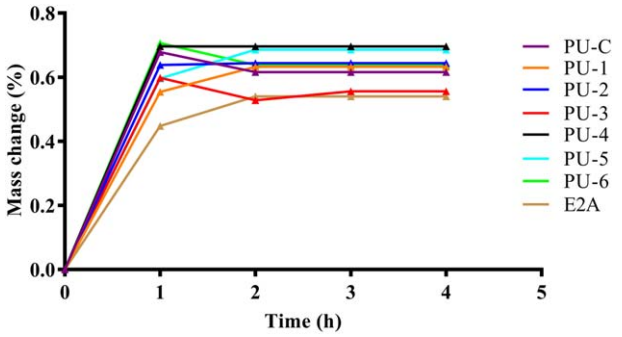

FIGURE 8. Water uptake of SiPUU and E2A as function of time at 37°C.

biodegradation of PU increases with the hydrophilicity as water accelerates the hydrolytic degradation.[37] E2A is successfully used in cardiovascular applications and it has been shown that the PU containing polyether SS absorb approximately twice the amount of water than E2A.[38] These SiPUU have comparable water uptake as E2A and this low water absorbance indicates their hydrophobic nature which agrees well with the CA data. Siloxane units in PDMS enhanced the hydrophobicity and minimized water uptake in SiPUU.[39]

CONCLUSION

We have demonstrated that incorporation of linked macrodiols with diisocyanate in synthesis of SiPUU enabled the development of materials with high mechanical strength and improved creep resistance. These SiPUU had surface enrichment with siloxane segments creating a hydrophobic surface and water uptake $<0.7\%$ of their dry mass. These improvements were observed for the SiPUU containing linked PHMO, the minor component of the SS. On the other hand, linking of PDMS, the major component of the SS did not have a significant effect on these properties. XPS results confirmed an increased presence of siloxane segments on the surface compared to bulk in SiPUU. AFM imaging showed that PU-1 based on MDI linked PHMO had the lowest surface adhesion, even when hydrated, confirming the siloxane-rich surface morphology. WAXS data suggested that there is a higher degree of short range interdomain ordering between the hard and soft domains. Overall, the SiPUU based on MDI linked PHMO had several favorable properties for it to be considered as a choice of material for fabrication of synthetic heart valve leaflets.

ACKNOWLEDGMENT

The authors would like to express their great appreciation to Frank McGuire, the Chief Executive of Foldax Inc. for providing the financial support to the first author. We also like to acknowledge Dr Ajay Padsalgikar of Abbott for providing E2A. We extend our appreciation to Malisja de Vries and Mark Greaves for helping with SEM-EDX experiments.

REFERENCES

1. Zdrahala RJ, Zdrahala IJ. Biomedical applications of polyurethanes: A review of past promises, present realities, and a vibrant future. J Biomater Appl 1999;14:67–90.
2. Gunatillake PA, Martin DJ, Meijs GF, Mccarthy SJ, Adhikari R. Designing biostable polyurethane elastomers for biomedical implants. Aust J Chem 2003;56:545–557.
3. Wu L, Weisberg DM, Runt J, Felder G, Snyder AJ, Rosenberg G. An investigation of the in vivo stability of poly(ether urethaneurea) blood sacs. J Biomed Mater Res 1999;44:371–380.
4. Choi T, Masser KA, Moore E, Weksler J, Padsalgikar A, Runt J. Segmented polyurethanes derived from novel siloxane-carbonate soft segments for biomedical applications. J Polym Sci B: Polym Phys 2011;49:865–872.
5. Vilensky VA, Lipatov YS. A criterion for microphase separation in segmented polyurethane and polyurethane ureas. Polymer 1994; 35:3069–3074.
6. Bonart R, Muller EH. Phase separation in urethane elastomers as judged by low-angle x-ray-scattering. 1. Fundamentals. J Macromol Sci Phys 1974;B10:177–189.
7. Bonart R, Muller EH. Phase separation in urethane elastomers as judged by low-angle x-ray-scattering. 2. Experimental results. J Macromol Sci Phys 1974;B10:345–357.
8. Adhikari R, Gunatillake PA, Bown M. Effect of polydimethylsiloxane macrodiol molecular weight on properties and morphology of polyurethane and polyurethaneurea. J Appl Polym Sci 2003;90: 1565–1573.
9. Adhikari R, Gunatillake PA, Mccarthy SJ, Meijs CF. Mixed macrodiol-based siloxane polyurethanes: Effect of the comacrodiol structure on properties and morphology. J Appl Polym Sci 2000;78:1071–1082.
10. Adhikari R, Gunatillake PA, Mccarthy SJ, Meijs GF. Effect of chain extender structure on the properties and morphology of polyurethanes based on h12mdi and mixed macrodiols (pdms-phmo). J Appl Polym Sci 1999;74:2979–2989.
11. Adhikari R, Gunatillake PA, Mccarthy SJ, Meijs GF. Low-modulus siloxane-based polyurethanes. I. Effect of the chain extender 1,3-bis(4-hydroxybutyl)1,1,3,3-tetramethyidisiloxane (bhtd) on properties and morphology. J Appl Polym Sci 2002;83:736–746.
12. Zha LS, Wu MY, Yang JJ. Hydrogen bonding and morphological structure of segmented polyurethanes based on hydroquinone-bis(beta-hydroxyethy)ether as a chain extender. J Appl Polym Sci 1999;73:2895–2902.
13. Yilgor I, Yilgor E, Wilkes GL. Critical parameters in designing segmented polyurethanes and their effect on morphology and properties: A comprehensive review. Polymer 2015;58:A1–A36.
14. Wilkoff BL, Rickard J, Tkatchouk E, Padsalgikar AD, Gallagher G, Runt J. The biostability of cardiac lead insulation materials as assessed from long-term human implants. J Biomed Mater Res Part B: Appl Biomater 2016;104:411–421.
15. Cosgriff-Hernandez E, Tkatchouk E, Touchet T, Sears N, Kishan A, Jenney C, Padsalgikar AD, Chen E. Comparison of clinical explants and accelerated hydrolytic aging to improve biostability assessment of silicone-based polyurethanes. J Biomed Mater Res Part A 2016;104:1805–1816.
16. Wheatley DJ, Raco L, Bernacca GM, Sim I, Belcher PR, Boyd JS. Polyurethane: Material for the next generation of heart valve prostheses? Euro J Card-Thorac Surg 2000;17:440–447.
17. Mackay TG, Wheatley DJ, Bernacca GM, Fisher AC, Hindle CS. New polyurethane heart valve prosthesis: Design, manufacture and evaluation. Biomaterials 1996;17:1857–1863.
18. Sheth JP, Yilgor E, Erenturk B, Ozhalici H, Yilgor I, Wilkes GL. Structure-property behavior of poly(dimethylsiloxane) based

segmented polyurea copolymers modified with poly(propylene oxide). Polymer 2005;46:8185–8193.
19. Sheth JP, Aneja A, Wilkes GL, Yilgor E, Atilla GE, Yilgor I, Beyer FL. Influence of system variables on the morphological and dynamic mechanical behavior of polydimethylsiloxane based segmented polyurethane and polyurea copolymers: A comparative perspective. Polymer 2004;45:6919–6932.
20. Hernandez R, Weksler J, Padsalgikar A, Runt J. Microstructural organization of three-phase polydimethylsiloxane-based segmented polyurethanes. Macromolecules 2007;40:5441–5449.
21. Gunatillake PA, Bown M, Adhikari R, Polyurethane/urea compositions. U.S. patent US20170119923-A1;May 04, 2017.
22. Dandeniyage LS, Gunatillake PA, Adhikari R, Bown M, Shanks R, Adhikari B. Development of high strength siloxane poly(urethane-urea) elastomers based on linked macrodiols for heart valve application. J Biomed Mater Res Part B: Appl Biomater 2017;00B: 000–000.
23. Yildirim E, Yurtsever M, Wilkes GL, Yilgor I. Effect of intersegmental interactions on the morphology of segmented polyurethanes with mixed soft segments: A coarse-grained simulation study. Polymer 2016;90:204–214.
24. Gallagher G, Padsalgikar A, Tkatchouk E, Jenney C, Iacob C, Runt J. Environmental stress cracking performance of polyether and pdms-based polyurethanes in an in vitro oxidation model. J Biomed Mater Res 2017;105:1544–1558.
25. Gu P, Nishida T, Fan ZH. The use of polyurethane as an elastomer in thermoplastic microfluidic devices and the study of its creep properties. Electrophoresis 2014;35:289–297.
26. Qi S, Yu M, Fu J, Li PD, Zhu M. Creep and recovery behaviors of magnetorheological elastomer based on polyurethane/epoxy resin ipns matrix. Smart Mater Struct 2016;25:10.
27. Wong S, Shanks R. Creep behaviour of biopolymers and modified flax fibre composites. Compos Interfaces 2008;15:131–145.
28. Yilgor E, Yilgor I. Silicone containing copolymers: Synthesis, properties and applications. Prog Polym Sci 2014;39: 1165–1195.
29. Askari F, Barikani M, Barmar M. Siloxane-based segmented poly(-urethane-urea) elastomer: Synthesis and characterization. J Appl Polym Sci 2013;130:1743–1751.
30. Liu JA, Pan ZQ, Gao Y. Study on the morphology structure and properties of aqueous polyurethane modified by poly(dimethyl siloxane). J Appl Polym Sci 2007;105:3037–3046.
31. Chattopadhyay DK, Sreedhar B, Raju K. Effect of chain extender on phase mixing and coating properties of polyurethane ureas. Ind Eng Chem Res 2005;44:1772–1779.
32. Hernandez R, Weksler J, Padsalgikar A, Runt J. In vitro oxidation of high polydimethylsiloxane content biomedical polyurethanes: Correlation with the microstructure. J Biomed Mater Res Part A 2008;87A:546–556.
33. Tyagi D, Mcgrath JE, Wilkes GL. Small-angle x-ray studies of siloxane-urea segmented copolymers. Polym Eng Sci 1986;26:1371–1398.
34. Velankar S, Cooper SL. Microphase separation and rheological properties of polyurethane melts. 2. Effect of block incompatibility on the microstructure. Macromolecules 2000;33:382–394.
35. Fredrickson GH, Milner ST, Leibler L. Multicritical phenomena and microphase ordering in random block copolymer melts. Macromolecules 1992;25:6341–6354.
36. Choi T, Weksler J, Padsalgikar A, Runt J. Influence of soft segment composition on phase-separated microstructure of polydimethylsiloxane-based segmented polyurethane copolymers. Polymer 2009;50:2320–2327.
37. Gorna K, Gogolewski S. In vitro degradation of novel medical biodegradable aliphatic polyurethanes based on -caprolactone and pluronics® with various hydrophilicities. Polym Degrad Stab 2002;75:113–122.
38. Chaffin KA, Buckalew AJ, Schley JL, Chen XJ, Jolly M, Alkatout JA, Miller JP, Untereker DF, Hillmyer MA, Bates FS. Influence of water on the structure and properties of pdms-containing multiblock polyurethanes. Macromolecules 2012;45:9110–9120.
39. Yu YJ, Infanger S, Grunlan MA, Maitland DJ. Silicone membranes to inhibit water uptake into thermoset polyurethane shape-memory polymer conductive composites. J Appl Polym Sci 2014; 132:41226, DOI: 10.1002/app.41226.